Coupling Matrix Representation of Nonreciprocal Filters Based on Time Modulated Resonators

Alejandro Alvarez-Melcon, *Senior Member, IEEE,* Xiaohu Wu, *Senior Member, IEEE,* Jiawei Zang, Xiaoguang Liu, *Senior Member, IEEE,* and J. Sebastian Gomez-Diaz, *Senior Member, IEEE*

***Abstract*—This paper addresses the analysis and design of non-reciprocal filters based on time modulated resonators. We analytically show that time modulating a resonator leads to a set of harmonic resonators composed of the unmodulated lumped elements plus a frequency invariant element that accounts for differences in the resonant frequencies. We then demonstrate that harmonic resonators of different order are coupled through non-reciprocal admittance inverters whereas harmonic resonators of the same order couple with the admittance inverter coming from the unmodulated filter network. This coupling topology provides useful insights to understand and quickly design non-reciprocal filters and permits their characterization using an asynchronously tuned coupled resonators network together with the coupling matrix formalism. Two designed filters, of orders three and four, are experimentally demonstrated using quarter wavelength resonators implemented in microstrip technology and terminated by a varactor on one side. The varactors are biased using coplanar waveguides integrated in the ground plane of the device. Measured results are found to be in good agreement with numerical results, validating the proposed theory.**

***Index Terms*—Coupling matrix, microwave filters, non reciprocity, spatio-temporal modulation, time modulated capacitors.**

I. Introduction

NON-RECIPROCAL components are of key importance in many electronic systems, such as radar or mobile and satellite communications [1]. Traditionally, such components have relied on magnetic materials, such as ferrites, under strong biasing fields. Increasingly stringent technological demands, in constant pursuit of integration, affordability, and miniaturization, have triggered the recent emergence of magnetless non-reciprocal approaches to break the Lorentz reciprocity principle [2] and the subsequent development of devices such as circulators [3]–[13], isolators [14]–[20], and even non-reciprocal leaky-wave antennas [21]–[23] operating in the absence of magneto-optical effects.

In this context, the concept of non-reciprocal filters based on time-modulated resonators have recently been put forward [24]. The operation principle behind this type of filters relies on tailoring the non-reciprocal power transfer among the RF and intermodulation frequencies to create constructive/destructive interferences at the input/output ports. The filters were analyzed in [24] through a dedicated spectral domain method combined with $ABCD$ parameters, and useful design guidelines on how to optimize the frequency, amplitude, and phase delay of the signals that modulate the resonators were given. A practical prototype was also experimentally demonstrated using varactors and lumped inductors.

In this paper, we develop a coupling matrix representation of non-reciprocal filters based on time modulated resonators. Starting from the initial unmodulated equivalent circuit, a multi-harmonic equivalent network is rigorously derived, taking into account the nonlinear harmonics (also known as intermodulation products) that are internally excited. By introducing the concept of harmonic resonators, the resulting structure is represented with a simple network based on a specific coupled resonator topology. It is analytically shown that resonators of identical harmonic orders are coupled with the admittance inverters found in the original unmodulated network while resonators of different harmonic orders are coupled through non-reciprocal admittance inverters. In addition, analytic formulas are derived to represent the new harmonic resonators with frequency invariant susceptances [25], [26] that account for differences in the resonant frequencies. In this way, all the resonators of the resulting network are expressed in terms of the original unmodulated resonators.

It is important to emphasize that the analytic calculation of the non-reciprocal admittance inverters and frequency invariant susceptances for harmonic resonators, together with the derived coupling topology, permits to analyze and design non-reciprocal filters using an asynchronously tuned coupled resonator network and the classical coupling matrix formalism [26]. Here the term *asynchronously tuned* is used to refer to coupling topologies having resonators tuned at different resonant frequencies. The formalism permits to easily consider filters of any order with an arbitrary number of nonlinear harmonics. As detailed below, this approach also sheds light on the underlying mechanisms that enable non-reciprocal responses in time-modulated filters. Besides filters operating at identical input/output frequencies, this technique can also be applied to analyze devices that exhibit non-reciprocity

Manuscript received Month DD, YYYY; revised Month DD, YYYY; accepted Month DD, YYYY.

This work is supported in part by the National Science Foundation with CAREER Grant No. ECCS-1749177 and by the grants PRX18/00092 and TEC2016-75934-C4-4-R of MECD, Spain.

A. A. Melcon was on sabbatical in the Department of Electrical and Computer Engineering at UC Davis. He is now with the Department of Information and Communication Technologies, Technical University Cartagena, 30202, Spain. e-mail: alejandro.alvarez@upct.es.

X. Wu is with the Department of Electrical and Computer Engineering, University of California, Davis, USA. e-mail: wxhwu@ucdavis.edu

J. Zang was a visiting student in the Department of Electrical and Computer Engineering at UC Davis. He is now with the School of Information and Electronics, Beijing Institute of Technology, Beijing 100081, China.

J. S. Gomez-Diaz and X. Liu are with the Department of Electrical and Computer Engineering, University of California, Davis, USA. e-mail: {jsgomez, lxgliu}@ucdavis.edu

between the fundamental frequency and desired nonlinear harmonics. Compared to the $ABCD$ approach presented in [24], the analysis techniques developed in this paper provides further insight into the frequency conversion dynamics of non-reciprocal filters based on time modulated resonators. This insight is reinforced with the derivation of a new equivalent network based on coupled resonators that accurately represent the dynamics of time modulated circuits, together with the development of the corresponding coupling matrix formalism. We have employed the guidelines proposed in [24] to design the non-reciprocal filters tested in this work.

After a review of the equivalent network for coupled resonators filters in Section II, we introduce in Section III the coupling matrix formalism for time-modulated filters. Numerical studies are first presented, including the convergence behavior of the scattering parameters with the number of harmonics. To demonstrate the usefulness of the proposed approach, in Section IV we present the design of two non-reciprocal filters of third and fourth orders. The filters are then experimentally demonstrated in Section V using quarter wavelength resonators implemented in microstrip technology. Coupled microstrip lines are terminated with varactors on one side to build time modulated resonators. A compact structure is obtained by integrating the feeding network of the modulating signal in the same board as the filter. This is achieved by using a coplanar waveguide feeding network in the ground plane of the device. Numerical results obtained with the theory presented in this paper show very good agreement with respect to measurements obtained from the manufactured prototypes.

II. Equivalent Network of Coupled Resonators Filters

Let us start from the basic ideal equivalent network of a lossless in-line filter represented by lumped elements and admittance inverters as shown in Fig. 1.

Fig. 1(a) shows the normalized lowpass filter prototype with all capacitors normalized to 1 F and the source and load impedances normalized to $1\,\Omega$ For the sake of clarity, but without loss of generality, we consider a network composed of three resonators (network of order $N = 3$). The $N + 2$ coupling matrix can be used to characterize this network [26], leading to

$$\underline{\underline{M}} = \begin{pmatrix} 0 & M_{P_1 1} & 0 & 0 & 0 \\ M_{P_1 1} & M_{11} & M_{12} & 0 & 0 \\ 0 & M_{12} & M_{22} & M_{23} & 0 \\ 0 & 0 & M_{23} & M_{33} & M_{3P_2} \\ 0 & 0 & 0 & M_{3P_2} & 0 \end{pmatrix}. \quad (1)$$

Here we have used the notation P_1 and P_2 to refer to the source S and load L terminations. This notation will be more convenient when investigating the non-reciprocal behavior of the network in the next section. Note that in this matrix the diagonal elements ($M_{u,u}$ with $u = 1, 2, \cdots, N$) represent the frequency invariant susceptances shown in Fig. 1(a), while the off-diagonal elements $M_{u,u+1}$ represent the values of the admittance inverters of the network. Frequency invariant susceptances are used in Fig. 1 to account for asynchronously tuned topologies [26].

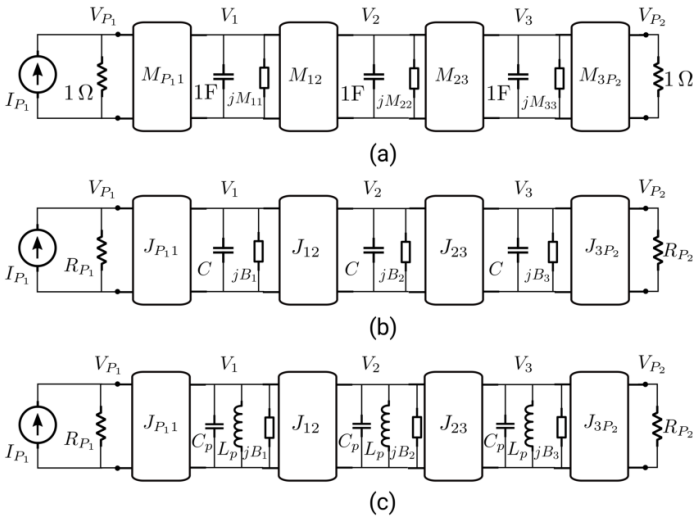

Fig. 1. Equivalent circuit of an ideal lossless filter based on lumped elements and admittance inverters. (a) Normalized lowpass prototype with all elements having unitary values. (b) Lowpass prototype scaled to arbitrary capacitance values C and port impedances R_{P_1}, R_{P_2}. (c) Bandpass network resulting from a standard lowpass to bandpass transformation.

This coupling matrix relates the currents and nodal voltages in the normalized network shown in Fig. 1(a). The Kirchhoff's current law in this network can be written in matrix form as

$$\underline{I} = \left[\underline{\underline{G}} + j\,\omega\,\underline{\underline{C}} + j\,\underline{\underline{M}}\right] \cdot \underline{V}, \quad (2)$$

where the whole admittance matrix has been expressed as the sum of three simpler matrices. In this expression $\underline{\underline{C}}$ is a matrix containing the capacitors of the network

$$\underline{\underline{C}} = \begin{pmatrix} 0 & 0 & 0 & 0 & 0 \\ 0 & C & 0 & 0 & 0 \\ 0 & 0 & C & 0 & 0 \\ 0 & 0 & 0 & C & 0 \\ 0 & 0 & 0 & 0 & 0 \end{pmatrix} \quad (3)$$

and $\underline{\underline{G}}$ is the so called conductance matrix, which contains the port admittances as

$$\underline{\underline{G}} = \begin{pmatrix} G_{P_1} & 0 & 0 & 0 & 0 \\ 0 & 0 & 0 & 0 & 0 \\ 0 & 0 & 0 & 0 & 0 \\ 0 & 0 & 0 & 0 & 0 \\ 0 & 0 & 0 & 0 & G_{P_2} \end{pmatrix}. \quad (4)$$

In the network shown in Fig. 1(a), the values $C = 1$ F, $G_{P_1} = 1/R_{P_1} = 1\,\Omega^{-1}$, and $G_{P_2} = 1/R_{P_2} = 1\,\Omega^{-1}$ are employed. Besides, in the system of equations described in (2), $\underline{I}$ represents the current excitation vector and $\underline{V}$ contains the unknown nodal voltages [see Fig. 1(a)], as

$$\underline{I} = \begin{pmatrix} I_{P_1} \\ 0 \\ 0 \\ 0 \\ 0 \end{pmatrix}, \quad \underline{V} = \begin{pmatrix} V_{P_1} \\ V_1 \\ V_2 \\ V_3 \\ V_{P_2} \end{pmatrix}. \quad (5)$$

From this normalized network, a scaled lowpass circuit as shown in Fig. 1(b) can be obtained. Capacitors and port impedances are scaled to arbitrary values C and $R_{P_1} =$

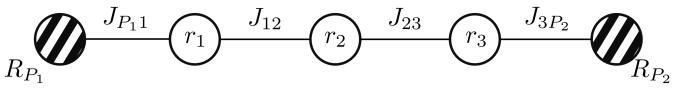

Fig. 2. Coupling topology of the in-line filter shown in Fig. 1.

$1/G_{P_1}$, $R_{P_2} = 1/G_{P_2}$, respectively. Note that during the production of a particular filter, the transformation ratios C are calculated with the information of the practical technology that will be used during the filter implementation.

In any case, the response of the scaled network is the same as the original network if the values of the admittance inverters $J_{u,u+1}$ and frequency invariant susceptances B_u are conveniently scaled as

$$J_{P_1 1} = M_{P_1 1}\sqrt{G_{P_1}\,C}, \qquad J_{u,u+1} = M_{u,u+1}\,C, \tag{6a}$$

$$J_{NP_2} = M_{NP_2}\sqrt{C\,G_{P_2}}, \qquad B_u = M_{u,u}\,C, \tag{6b}$$

If a standard lowpass to bandpass transformation is applied to the network of Fig. 1(b), the capacitors are transformed into resonators, thus obtaining the traditional bandpass network shown in Fig. 1(c). In this network all resonators are equal and take the values

$$C_p = \frac{C}{\omega_0\,F_B}, \qquad L_p = \frac{F_B}{\omega_0\,C} = \frac{1}{\omega_0^2\,C_p}, \tag{7a}$$

$$F_B = \frac{\omega_{c2} - \omega_{c1}}{\omega_0}, \qquad \omega_0 = 2\,\pi\,f_0, \tag{7b}$$

where f_0 is the center frequency of the passband and ω_{c1} and ω_{c2} are the lower and upper angular equi-ripple cut-off frequencies of the passband, respectively.

The network shown in Fig. 1(c) represents a bandpass filter with the so called in-line coupling topology, as illustrated in Fig. 2. In this figure, white circles represent the resonators of the structure r_u, while dashed circles represent the terminal ports with reference impedances $R_{P_1} = 1/G_{P_1}$, $R_{P_2} = 1/G_{P_2}$. Also, solid lines connecting the circles represent the ideal admittance inverters of the network $J_{P_1 1}$, $J_{u,u+1}$, J_{NP_2}.

If Kirchhoff's current law is applied to the nodes of the bandpass network shown in Fig. 1(c), the following linear system of equations is obtained

$$\begin{pmatrix} I_{P_1} \\ 0 \\ 0 \\ 0 \\ 0 \end{pmatrix} = \begin{pmatrix} G_{P_1} & jJ_{P_1 1} & 0 & 0 & 0 \\ jJ_{P_1 1} & Y_p^{(1)} & jJ_{12} & 0 & 0 \\ 0 & jJ_{12} & Y_p^{(2)} & jJ_{23} & 0 \\ 0 & 0 & jJ_{23} & Y_p^{(3)} & jJ_{3P_2} \\ 0 & 0 & 0 & jJ_{3P_2} & G_{P_2} \end{pmatrix} \cdot \begin{pmatrix} V_{P_1} \\ V_1 \\ V_2 \\ V_3 \\ V_{P_2} \end{pmatrix} \tag{8}$$

where $Y_p^{(u)}$ is the admittance of the resonators, calculated as

$$Y_p^{(u)} = j\,\omega\,C_p + \frac{1}{j\,\omega\,L_p} + j\,B_u. \tag{9}$$

Similarly as before, it is now convenient to express the matrix of the system as the sum of three matrices as

$$\underline{I} = \left[\underline{\underline{G}} + \underline{\underline{Y_{inv}}} + \underline{\underline{Y_p}}\right] \cdot \underline{V}. \tag{10}$$

The first matrix is again the conductance matrix defined in (4). The second matrix is symmetric and contains the values of the admittance inverters of the network

$$\underline{\underline{Y_{inv}}} = j \begin{pmatrix} 0 & J_{P_1 1} & 0 & 0 & 0 \\ J_{P_1 1} & 0 & J_{12} & 0 & 0 \\ 0 & J_{12} & 0 & J_{23} & 0 \\ 0 & 0 & J_{23} & 0 & J_{3P_2} \\ 0 & 0 & 0 & J_{3P_2} & 0 \end{pmatrix}. \tag{11}$$

Finally, the third matrix represents the admittances of the resonators

$$\underline{\underline{Y_p}} = \begin{pmatrix} 0 & 0 & 0 & 0 & 0 \\ 0 & Y_p^{(1)} & 0 & 0 & 0 \\ 0 & 0 & Y_p^{(2)} & 0 & 0 \\ 0 & 0 & 0 & Y_p^{(3)} & 0 \\ 0 & 0 & 0 & 0 & 0 \end{pmatrix}. \tag{12}$$

Note that the size of all these matrices is the same as that of the regular coupling matrix with ports, namely $(N+2) \times (N+2)$. Also, we want to remark that the admittance inverters are located in the off diagonal elements of (11), and that the information of the resonators appears in the diagonal entries of (12). We stress that all matrices involved in the formulation are symmetric, therefore assuring that the considered network is completely reciprocal.

III. Network with Time Modulated Resonators

Applying time-varying signals to modulate the capacitors of the bandpass network shown in Fig. 1 makes the system nonlinear [27], [28]. In this work, we will consider that the values of the capacitors are modulated in time with the following sinusoidal variation

$$C_p^{(u)}(t) = C_p\left[1 + \Delta_m\,\cos(\omega_m\,t + \varphi_u)\right], \tag{13}$$

where ω_m is the angular frequency of the modulating signal, φ_u is the initial phase, and Δ_m is the modulation index. Even though we will use the same modulation frequency and modulation index to modulate all capacitors, their initial phases may be different along the network, i.e., $\varphi_u = (u-1)\,\Delta_\varphi$ with $u = 1, 2, \cdots, N$. It will be shown later in this paper that this phase difference is the key mechanism that enables non-reciprocal responses.

In this scenario, a number of nonlinear harmonics N_{har} are generated in each resonator, resulting into the equivalent network shown in Fig. 3. These nonlinear harmonics are coupled by the time modulated capacitors. For simplicity, the figure only shows $N_{har} = 3$ harmonics (i.e., $k = \cdots, -1, 0, 1, \cdots$ with k denoting the order of a given nonlinear harmonic).

The application of Kirchhoff's current law on the network shown in Fig. 3 leads to a linear system with a structure very similar to the one given in (10). However, each entry in the matrix system becomes now a submatrix of size $N_{har} \times N_{har}$ due to the generated nonlinear harmonics. In this way, the

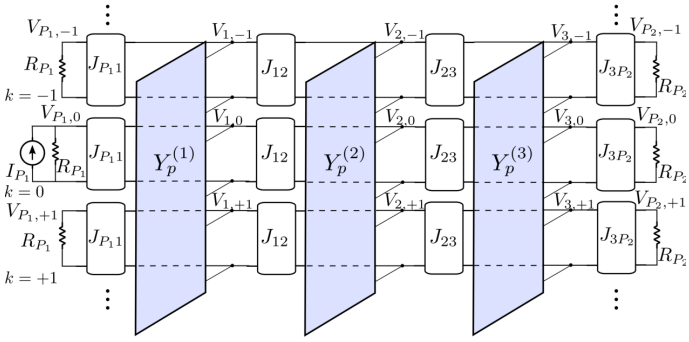

Fig. 3. Equivalent circuit of the ideal filter shown in Fig. 1(c) when a time domain signal is used to modulate the value of the capacitors. Color boxes represent the admittance coupling matrix between generated harmonics.

vector containing the nodal voltages becomes

$$\underline{V} = \begin{pmatrix} \underline{V_{P_1}} \\ \underline{V_1} \\ \underline{V_2} \\ \underline{V_3} \\ \underline{V_{P_2}} \end{pmatrix}, \qquad \underline{V_{P_1}} = \begin{pmatrix} V_{P_1,-2} \\ V_{P_1,-1} \\ V_{P_1,0} \\ V_{P_1,+1} \\ V_{P_1,+2} \end{pmatrix}, \tag{14a}$$

$$\underline{V_u} = \begin{pmatrix} V_{u,-2} \\ V_{u,-1} \\ V_{u,0} \\ V_{u,+1} \\ V_{u,+2} \end{pmatrix}, \qquad \underline{V_{P_2}} = \begin{pmatrix} V_{P_2,-2} \\ V_{P_2,-1} \\ V_{P_2,0} \\ V_{P_2,+1} \\ V_{P_2,+2} \end{pmatrix}, \tag{14b}$$

where the number of harmonics considered is five ($N_{har} = 5$, $k = \cdots, -2, -1, 0, 1, 2, \cdots$) and the total number of unknowns in the system of linear equations becomes $(N + 2)\, N_{har}$. We recall that in our notation u is an integer sweeping the physical resonators ($u = 1, 2, \cdots N$). Therefore $\underline{V_u}$ of (14b) are simply the 2 to $N+1$ entries of $\underline{V}$ shown in (14a). Then, following the same strategy as before, the conductance matrix is written as

$$\underline{\underline{G}} = \begin{pmatrix} \underline{\underline{G_{P_1}}} & \underline{\underline{0}} & \underline{\underline{0}} & \underline{\underline{0}} & \underline{\underline{0}} \\ \underline{\underline{0}} & \underline{\underline{0}} & \underline{\underline{0}} & \underline{\underline{0}} & \underline{\underline{0}} \\ \underline{\underline{0}} & \underline{\underline{0}} & \underline{\underline{0}} & \underline{\underline{0}} & \underline{\underline{0}} \\ \underline{\underline{0}} & \underline{\underline{0}} & \underline{\underline{0}} & \underline{\underline{0}} & \underline{\underline{0}} \\ \underline{\underline{0}} & \underline{\underline{0}} & \underline{\underline{0}} & \underline{\underline{0}} & \underline{\underline{G_{P_2}}} \end{pmatrix}, \tag{15}$$

where $\underline{\underline{0}}$ denotes the zero matrix. The other sub-matrices are diagonal and represent the loads to the new generated harmonics as $\underline{\underline{G_{P_1}}} = G_{P_1}\, \underline{\underline{U}}$ and $\underline{\underline{G_{P_2}}} = G_{P_2}\, \underline{\underline{U}}$, with $\underline{\underline{U}}$ being the identity matrix. In addition, the matrix of the admittance inverters can now be written as

$$\underline{\underline{Y_{inv}}} = j \begin{pmatrix} \underline{\underline{0}} & \underline{\underline{J_{P_1 1}}} & \underline{\underline{0}} & \underline{\underline{0}} & \underline{\underline{0}} \\ \underline{\underline{J_{P_1 1}}} & \underline{\underline{0}} & \underline{\underline{J_{12}}} & \underline{\underline{0}} & \underline{\underline{0}} \\ \underline{\underline{0}} & \underline{\underline{J_{12}}} & \underline{\underline{0}} & \underline{\underline{J_{23}}} & \underline{\underline{0}} \\ \underline{\underline{0}} & \underline{\underline{0}} & \underline{\underline{J_{23}}} & \underline{\underline{0}} & \underline{\underline{J_{3P_2}}} \\ \underline{\underline{0}} & \underline{\underline{0}} & \underline{\underline{0}} & \underline{\underline{J_{3P_2}}} & \underline{\underline{0}} \end{pmatrix}, \tag{16}$$

where the submatrices $\underline{\underline{J_{u,u+1}}} = J_{u,u+1}\, \underline{\underline{U}}$ are also diagonal and represent the couplings of same order harmonics between the different resonators. Here we should remark that with the equivalent network employed, which uses ideal frequency independent inverters, the couplings of same order harmonics between different resonators are all identically affected by the original inverters. This is a narrowband approximation usually introduced in the theory of coupling matrices [26]. In real implementations, harmonics will be affected by the inverters in a slightly different way due to their intrinsic dispersive nature. These dispersive effects maybe important for wideband responses and special techniques may be needed to preserve accuracy [29], [30]. However, for narrowband responses (fractional bandwidths typically less than 15%), the narrowband approximation usually gives good results [26].

Finally, the matrix that contains the resonator admittances becomes

$$\underline{\underline{Y_p}} = \begin{pmatrix} \underline{\underline{0}} & \underline{\underline{0}} & \underline{\underline{0}} & \underline{\underline{0}} & \underline{\underline{0}} \\ \underline{\underline{0}} & \underline{\underline{Y_p^{(1)}}} & \underline{\underline{0}} & \underline{\underline{0}} & \underline{\underline{0}} \\ \underline{\underline{0}} & \underline{\underline{0}} & \underline{\underline{Y_p^{(2)}}} & \underline{\underline{0}} & \underline{\underline{0}} \\ \underline{\underline{0}} & \underline{\underline{0}} & \underline{\underline{0}} & \underline{\underline{Y_p^{(3)}}} & \underline{\underline{0}} \\ \underline{\underline{0}} & \underline{\underline{0}} & \underline{\underline{0}} & \underline{\underline{0}} & \underline{\underline{0}} \end{pmatrix}. \tag{17}$$

Each admittance submatrix represents the coupling among the different nonlinear harmonics generated in a resonator with a time-modulated capacitor.

Applying the theory reported in [31], [32], which assumes ideal capacitors, permits to express each of these submatrices as

$$\underline{\underline{Y_p^{(u)}}} = \underline{\underline{Y_b}} + j\, \underline{\underline{\omega_n}}\, \underline{\underline{N_c^{(u)}}} + j\, B_u\, \underline{\underline{U}}, \tag{18}$$

where $\underline{\underline{\omega_n}}$ is a diagonal matrix containing the angular frequencies of the nonlinear harmonics (spectral matrix), namely

$$\underline{\underline{\omega_n}} = \begin{pmatrix} \omega - 2\omega_m & 0 & 0 & 0 & 0 \\ 0 & \omega - \omega_m & 0 & 0 & 0 \\ 0 & 0 & \omega & 0 & 0 \\ 0 & 0 & 0 & \omega + \omega_m & 0 \\ 0 & 0 & 0 & 0 & \omega + 2\omega_m \end{pmatrix}. \tag{19}$$

The matrix $\underline{\underline{Y_b}}$ includes the presence of the inductors in the modulated resonators and can be expressed as

$$\underline{\underline{Y_b}} = \frac{1}{j\, L_p}\, \underline{\underline{\omega_n}}^{-1}. \tag{20}$$

Finally, $\underline{\underline{N_c^{(u)}}}$ models how the nonlinear harmonics are excited due to the modulated capacitors and it can be written as

$$\underline{\underline{N_c^{(u)}}} = \begin{pmatrix} C_p & D^{(u)} & 0 & 0 & 0 \\ E^{(u)} & C_p & D^{(u)} & 0 & 0 \\ 0 & E^{(u)} & C_p & D^{(u)} & 0 \\ 0 & 0 & E^{(u)} & C_p & D^{(u)} \\ 0 & 0 & 0 & E^{(u)} & C_p \end{pmatrix}. \tag{21}$$

The new elements of this matrix depend on the modulation index and on the phases of the modulating signal as

$$D^{(u)} = \frac{\Delta_m\, C_p}{2}\, e^{-j\, \varphi_u}, \qquad E^{(u)} = \frac{\Delta_m\, C_p}{2}\, e^{+j\, \varphi_u}. \tag{22}$$

By doing straightforward operations with these matrices, the final admittance submatrix in (18) can be written as shown in (23) (top of the next page). In this last expression, we have

$$\underline{\underline{Y_p^{(u)}}} = \begin{pmatrix} Y_r^{(-2)} + jB_u & jD^{(u)}\,(\omega - 2\omega_m) & 0 & 0 & 0 \\ jE^{(u)}\,(\omega - \omega_m) & Y_r^{(-1)} + jB_u & jD^{(u)}\,(\omega - \omega_m) & 0 & 0 \\ 0 & jE^{(u)}\,\omega & Y_r^{(0)} + jB_u & jD^{(u)}\,\omega & 0 \\ 0 & 0 & jE^{(u)}\,(\omega + \omega_m) & Y_r^{(+1)} + jB_u & jD^{(u)}\,(\omega + \omega_m) \\ 0 & 0 & 0 & jE^{(u)}\,(\omega + 2\omega_m) & Y_r^{(+2)} + jB_u \end{pmatrix} \tag{23}$$

employed the following auxiliary admittance

$$Y_r^{(k)} = j\,C_p\left(\omega + k\,\omega_m\right) + \frac{1}{j\,L_p\left(\omega + k\,\omega_m\right)}. \tag{24}$$

The form of the matrix shown in (23) admits an interesting interpretation of the nonlinear phenomenon in terms of coupled network resonators. Following the coupling matrix formalism, the elements in the diagonal represent new resonators due to the generated nonlinear harmonics that we denote as harmonic resonators. Therefore, each physically modulated resonator gives rise to N_{har} new harmonic resonators yielding to a network of order $N_{har}\,N$. These resonators have different resonant frequencies, transforming the original structure into an asynchronously tuned coupled resonators network.

The resonant frequencies of the new harmonic resonators can be obtained by equating the diagonal elements of the matrix shown in (23) to zero. However, following the coupling matrix formalism, it would be convenient to formulate all resonators to be equal and employ additional frequency invariant susceptances to account for differences in the resonant frequencies. This can be accomplished by first writing (24) as

$$Y_r^{(k)} = j\,\omega\,C_p + j\,C_p\,k\,\omega_m + \frac{1}{j\,\omega\,L_p\Big(1 + k\,\omega_m/\omega\Big)}, \tag{25}$$

and then applying the following Taylor expansion

$$\frac{1}{1+x} \approx 1 - x + \cdots, \qquad x < 1 \tag{26}$$

to the third term to obtain

$$Y_r^{(k)} \approx j\,\omega\,C_p + \frac{1}{j\,\omega\,L_p} + j\left(C_p\,k\,\omega_m + \frac{k\,\omega_m}{\omega^2\,L_p}\right). \tag{27}$$

Note that this Taylor expansion can be used in this context since, in general, we assume that the modulation frequency is significantly smaller than the operation frequency, i.e., $\omega_m << \omega$ [24].

The comparison of this expression with (9) shows that the harmonic resonators can be made all equal to the static resonators in the unmodulated network. The differences in resonant frequencies can be modeled with additional frequency invariant susceptances, defined as

$$\hat{B}_k = C_p\,k\,\omega_m + \frac{k\,\omega_m}{\omega_0^2\,L_p}, \tag{28}$$

where, in order to make the frequency invariant susceptances truly independent on frequency, the center frequency of the passband ω_0 has been used in the last definition. The approximation will remain valid for narrowband filters. These frequency invariant susceptances can also be formulated in terms of the initial lowpass capacitors as

$$\hat{B}_k = \frac{2\,k\,\omega_m\,C}{\omega_0\,F_B}. \tag{29}$$

It can be observed that the frequency invariant susceptances associated to harmonic resonators depend on the order of the nonlinear harmonic itself k, on the modulation frequency ω_m and on the passband bandwidth. This expression is also very useful, since it will directly translate into the diagonal elements of the coupling matrix for the non-reciprocal filter by setting the lowpass capacitor to unity, i.e., $C = 1$ F.

It is illustrative to compare the structure of the matrices shown in (8) and in (23). Specifically, the off diagonal elements of the matrix (23) indicate that the new harmonic resonators are coupled following an in-line coupling topology among them. However, it can be observed that the matrix is not symmetric. This indicates that these harmonic resonators are coupled through non-reciprocal admittance inverters. Following this idea, we define a non-reciprocal admittance inverter to represent the coupling between two different harmonics $k-1$ and k, belonging to a specific physical resonator u, as

$$\begin{cases} J_u^{(k,k-1)} = D^{(u)}\,\big[\omega + k\,\omega_m\big], & \text{Low to up.} \\ J_u^{(k-1,k)} = E^{(u)}\,\big[\omega + (k-1)\,\omega_m\big], & \text{Up to low.} \end{cases} \tag{30}$$

so a coupling from a lower order harmonic to an upper order harmonic will use the top formula of (30), while a coupling from an upper order harmonic to a lower order harmonic will involve the bottom formula. An explicit expression for this non-reciprocal inverter can be obtained in the lowpass domain as

$$\begin{cases} J_u^{(k,k-1)} = \dfrac{\Delta_m}{2}\dfrac{C}{\omega_0\,F_B}\,e^{-j\varphi_u}\,\big[\omega_0 + k\,\omega_m\big] \\ J_u^{(k-1,k)} = \dfrac{\Delta_m}{2}\dfrac{C}{\omega_0\,F_B}\,e^{+j\varphi_u}\,\big[\omega_0 + (k-1)\,\omega_m\big] \end{cases} \tag{31}$$

where the center angular frequency of the passband has been used to define frequency invariant inverters.

We remark that these admittance inverters are different from those shown in (16). Admittance inverters in (16) come from the unmodulated network, and they couple same order harmonics between different physical resonators. On the contrary, these new admittance inverters play an important role in the nonlinear process occurring within each time modulated resonator. As a consequence, the new admittance inverters in (31) model the couplings between the different harmonics, generated, due to the nonlinear process, within the same physical resonator.

These last expressions indicate that the coupling between adjacent harmonic resonators belonging to a specific physical modulated capacitor can be controlled with the modulation

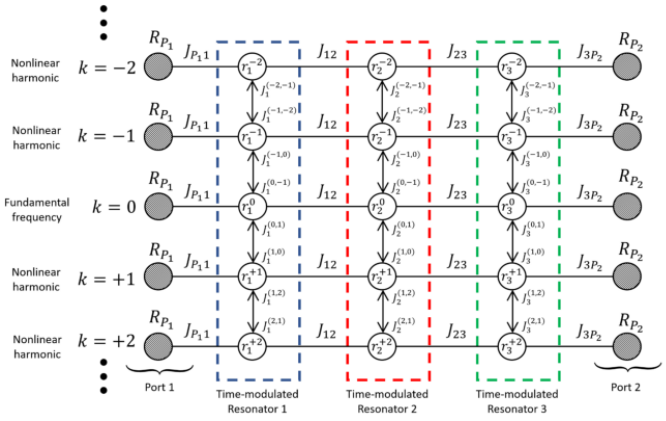

Fig. 4. Coupling topology of the in-line filter shown in Fig. 1(c) when the capacitors of the resonators are modulated with a time varying signal.

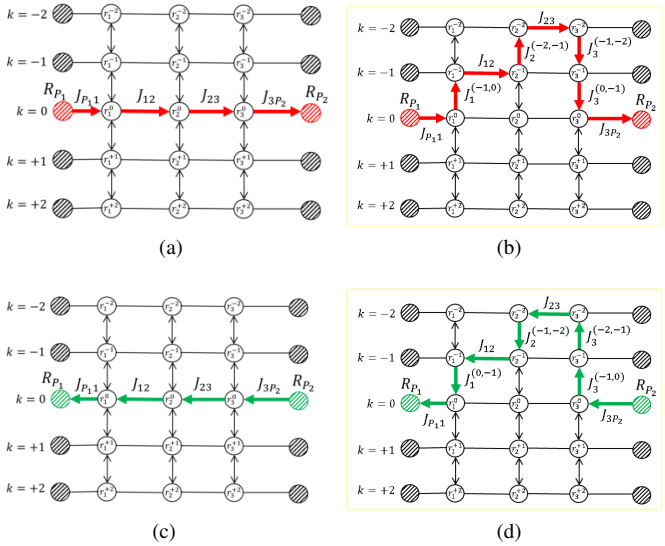

Fig. 5. Different paths that can be followed by electromagnetic waves to travel from port 1 to port 2 (top row) and from port 2 to port 1 (bottom row) in the coupling topology described in Fig. 4.

frequency ω_m, modulation index Δ_m, and initial phase of the modulation signal φ_u. Moreover, the degree of non-reciprocity of the coupling depends on both, the initial phase of the modulating signal and the modulation frequency. These expressions represent the values along the off-diagonal elements of the coupling matrix for the final non-reciprocal filter, once the value of the lowpass capacitor is set to unity ($C = 1$).

The analysis presented above permits an insightful interpretation of non-reciprocal filters in terms of an asynchronously tuned coupled resonators network. As already indicated, the order of the equivalent network is $N\,N_{har}$. Its coupling topology is further shown in Fig. 4. In this figure, harmonic resonators are identified with white circles as $r_u^{(k)}$. These harmonic resonators are defined with the same inductors L_p, capacitors C_p and frequency invariant susceptances B_u as the original static resonators. However, the new frequency invariant susceptances $\hat{B}_k$ given in (29) must be added to correctly represent their resonant frequencies. Furthermore, solid lines represent regular inverters modeling the couplings of same order harmonics between different physical resonators, as defined in (6). Finally, lines terminated in arrows represent non-reciprocal inverters modeling the couplings between different order harmonic resonators belonging to the same physical resonator, as defined in (30) or (31). It is also interesting to note that this coupled resonator network can easily be characterized with the traditional coupling matrix formalism [26], using the results obtained in this Section. In this case the size of the coupling matrix is $(N+2)N_{har} \times (N+2)N_{har}$.

It is interesting to note that according to the admittance inverters expressed in (31), the coupling strength increases with the order of the harmonics. This implies that the coupling towards higher order harmonics would be very strong, which is a somewhat counter-intuitive scenario. The situation, however, can be better understood with the coupling topology shown in Fig. 4. This topology explicitly states that coupling can only occur between contiguous harmonics, thus avoiding direct power coupling towards high-order harmonics.

Furthermore, the topology shown in Fig. 4 explicitly shows that the non-reciprocal response in time-modulated filters originates due to the non-reciprocal coupling [see (31)] between adjacent nonlinear harmonics that appear in time-modulated resonators. Following this scheme, the underlying non-reciprocal mechanism can be intuitively understood as follows. Electromagnetic waves propagating from port 1 can reach port 2 and keep the same oscillation frequency by (i) going through the admittance inverters that link the different resonators at the fundamental frequency, as in regular in-line filters (see Fig. 2 and Fig. 5a); and (ii) going through an ideally infinite number of routes (assuming an infinite number of nonlinear harmonics) that appear in the topology due to the presence of harmonic resonators. One specific example of these routes, illustrated in Fig. 5b, involves the harmonic admittance inverters $J_1^{(-1,0)}$, $J_2^{(-2,-1)}$, $J_3^{(-1,-2)}$, and $J_3^{(0,-1)}$ that impart a total phase of $+\varphi_1 + \varphi_2 - 2\varphi_3$ to the waves propagating therein. The output at port 2 is then conformed by the interference of the waves coming from all possible routes. Let us now consider the dual case, i.e., waves coming from port 2 and propagating towards port 1. As in our previous analysis, propagating waves can follow the path of common in-line filters (see Fig. 5c) plus potentially any of the ideally infinite routes enabled by harmonic resonators. The former leads to reciprocal contributions whereas any of the paths that encompasses nonlinear harmonics introduces non-reciprocity due to the non-reciprocal response of the impedance inverters. For instance, Fig. 5d shows the route previously analyzed but considering now the opposite propagation direction of the waves. This specific path involves the same harmonic impedance inverters as before, but traversed in the opposite direction, thus providing a total phase of $-\varphi_1 - \varphi_2 + 2\varphi_3$ to the waves (negative with respect to the previous scenario). For instance, assuming $\Delta_\varphi = 45°$, the total phase difference between forward and backward paths in this example is of $90°$. It is thus evident that an adequate control of the phase imparted by each time-modulated resonator is key to control the response of this type of filters. At port 1, waves

coming from all routes interfere to construct the output signal. Strong non-reciprocity at the same frequency arises due to the different wave interference that appears in ports 1 and 2.

The design of time-modulated non-reciprocal filters can be carried out following the guidelines described in [24]. In such design, the goal is to optimize the modulation frequency and index as well as the initial phase of the modulation signal applied to each resonator to (i) independently manipulate the interference of all waves that merge at ports 1 and 2 to boost non-reciprocity; (ii) maximize the energy coupled to nonlinear harmonics; and (iii) ensure that most energy is transferred back to the operation frequency at the device ports to minimize loss. It is important to remark that it is required to modulate at least two physical resonators to enable non-reciprocal responses [24]. If one modulates just a single resonator, the incoming energy will simply be distributed among various nonlinear harmonics that will then propagate through the network. Finally, note that we have focused here on non-reciprocal responses at the same frequency. It is indeed possible to design devices based on time-modulated resonators that exhibit non-reciprocal responses between the fundamental frequency and any desired nonlinear harmonic. These devices will be governed by the topology shown in Fig. 4 and will follow the theory developed above.

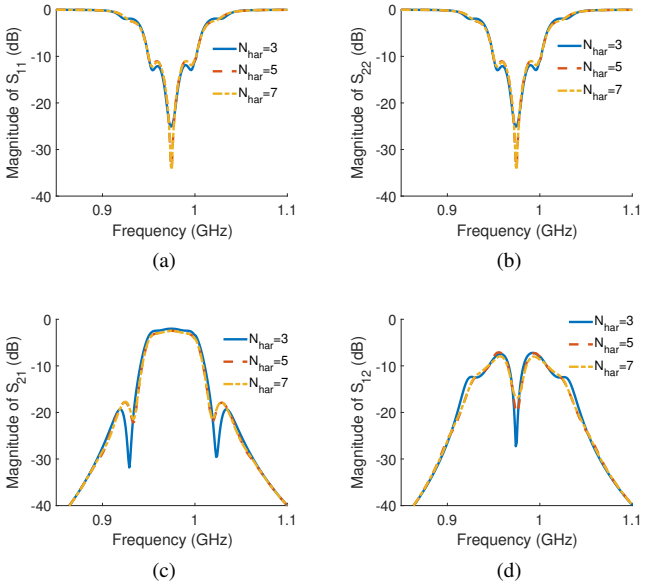

Fig. 6. Scattering parameters of the third order non-reciprocal filter designed in Section IV. Results are computed with the coupling matrix approach introduced in this work using an increasing number of harmonics in the numerical method.

IV. Numerical Results

Using the coupling matrix formalism derived above, a software tool for the analysis of non-reciprocal in-line filters has been developed. In this Section, we will investigate the convergence of the numerical algorithm as a function of the number of harmonics N_{har} included in the calculations.

The first example is a filter of order three whose unmodulated response has equal ripple return losses of $RL = 13$ dB. The filter coupling matrix yields

$$\underline{\underline{M_3}} = \begin{pmatrix} 0 & 0.8894 & 0 & 0 & 0 \\ 0.8894 & 0 & 0.8294 & 0 & 0 \\ 0 & 0.8294 & 0 & 0.8294 & 0 \\ 0 & 0 & 0.8294 & 0 & 0.8894 \\ 0 & 0 & 0 & 0.8894 & 0 \end{pmatrix}. \tag{32}$$

This coupling matrix gives the response of the normalized lowpass prototype.

The bandpass response is adjusted to have a bandwidth of 47 MHz, with a center frequency of $f_0 = 975$ MHz ($F_B = 4.8\%$). The modulation parameters were optimized, leading to the following values: $f_m = 22.8$ MHz, $\Delta_m = 0.050$, and $\Delta_\varphi = 35°$.

Here we should remark that the design of this filter is not yet completely determined by synthesis techniques. Rather, the coupling matrix shown in (32) gives the initial response of the unmodulated filter. Once this response is established, the parameters of the modulation signals are optimized to obtain the desired non-reciprocal response [24].

In general, the design of this filter fully from synthesis techniques would involve (i) the calculation of suitable reflection and transmission polynomials to properly represent the desired (non-reciprocal) transfer functions, (ii) the extraction from these polynomials of a suitable coupling matrix and (iii) the transformation of the obtained coupling matrix into a form that represents the coupling topology shown in Fig. 4.

Fig. 6 shows the scattering parameters at the fundamental frequency, obtained for this filter with increasing number of harmonics $N_{har} = 3, 5, 7$. Numerical results were obtained from the responses of the coupling matrices for the time modulated network. Such matrices are easily calculated starting with the coupling matrix given in (32) for the unmodulated network, and then considering the selected parameters for the modulation signal (f_m, Δ_m and Δ_φ). Next, using the coupling topology shown in Fig. 4, the coupling matrix entries for the time modulated network are computed with (29) and (31), with $C = 1$.

It can be observed that the results are in general very stable, showing only small differences as the number of harmonics is increased. Note that the algorithm converges using just $N_{har} = 5$ harmonics and increasing further the number of harmonics leads to negligible changes in the simulated response. Results show that the filter has a passband which is quite flat in the forward direction with a bandwidth of 48 MHz measured at the return loss level of 11 dB. It should be stressed that, even though the network is non-reciprocal it is symmetric and thus return losses from both ports are identical. Insertion losses within the passband in the forward direction are 2.5 dB. Since the network is lossless, these losses are in fact due to power that is converted to nonlinear harmonics and is not converted back to the fundamental frequency. In order to avoid such losses while preserving the integrity of wideband signals, i.e., preventing that nonlinear harmonics could interfere with signals propagating through the filter bandpass, it would be ideal to eliminate all higher order nonlinear harmonics at the ports. The resulting device would be a pseudo-linear time-

invariant filter in which nonlinear harmonics appear and propagate within the circuit but are completely cancelled at the ports. Such configuration has recently been put forward in the case of circulators composed of three ports [12]. The time-modulated filters proposed here are composed of only two ports, which decreases the degrees of freedom to construct pseudo-linear time-invariant devices. Specifically, in the forward direction, it is indeed desirable to completely eliminate higher order nonlinear harmonics at both ports, which in turn decreases the losses associated to the device. The situation is different when the port 2 is excited (backward direction). Since the proposed filter is a two port device, the power that is neither reflected nor transmitted must be transferred to higher order harmonics at the ports. Therefore, the goal would be to cancel out higher order harmonics at Port 1 while at the same time maximizing the power reflected back to high order harmonics at Port 2, thus achieving maximum isolation. We have observed that with the in-line topology studied in this paper, a complete cancellation of undesired higher order harmonics at the ports does not seem to be possible. We have verified that the power levels coupled to the strongest undesired higher order harmonics at the opposite ports are always below -9 dB. Further improvements might be possible by investigating differential arrangements similar to those described in [12].

In any case, Fig. 6 confirms that very strong non-reciprocity is obtained at the center of the passband, being the insertion loss of about 17 dB. Overall, the insertion losses in the backward direction are greater that 8 dB within the whole useful bandwidth. It should be noted that even though large isolation can be obtained at the center of the passband, it deteriorates at the edges of the useful bandwidth. As detailed in the previous section, non-reciprocity is obtained by provoking energy conversion from the fundamental frequency to nonlinear harmonics. Although these conversion effects are non-reciprocal in magnitude and phase, the main mechanism that allows to obtain high non-reciprocity is the difference in phase between the forward and backward paths. Therefore, high isolation is obtained by adjusting the phases among the resonators to produce phase cancellation effects in the backward direction. With a small number of resonators (three in this example), these cancellation effects can be made efficient only over a narrow bandwidth. Moreover, as it will be discussed in our next example, there is a trade-off between the isolation level and the bandwidth where this isolation is achieved.

If we define the directivity between the forward and backward directions as

$$D = \frac{|S_{21}|^2}{|S_{12}|^2}, \tag{33}$$

then a directivity of $D_0 = 14.5$ dB is obtained at center frequency. Moreover, the directivity within the useful passband is always better than $D = 5.5$ dB.

To demonstrate the convergence of the algorithm when the order of the network is increased, we have also designed a fourth order non-reciprocal filter. For this second example the return losses of the unmodulated filter are $RL = 18.5$ dB,

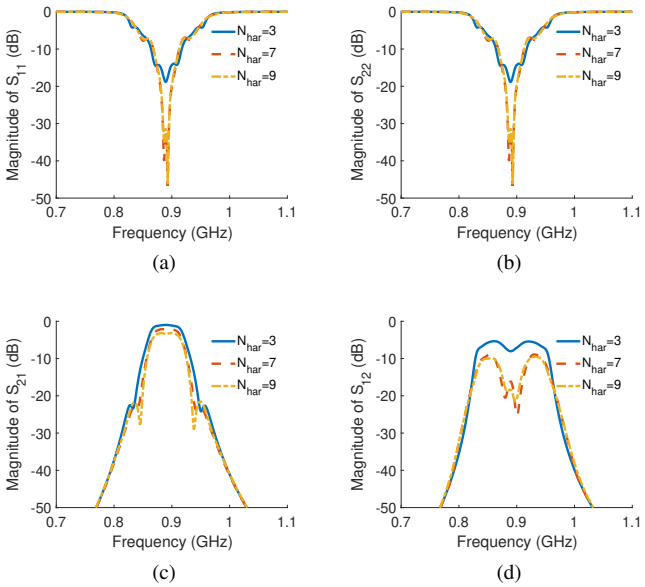

Fig. 7. Scattering parameters of the forth order non-reciprocal filter designed in Section IV. Results are computed with the coupling matrix approach introduced in this work using an increasing number of harmonics in the numerical method.

leading to the following coupling matrix

$$\underline{\underline{M_4}} = \begin{pmatrix} 0 & 0.997 & 0 & 0 & 0 & 0 \\ 0.997 & 0 & 0.873 & 0 & 0 & 0 \\ 0 & 0.873 & 0 & 0.68 & 0 & 0 \\ 0 & 0 & 0.68 & 0 & 0.873 & 0 \\ 0 & 0 & 0 & 0.873 & 0 & 0.997 \\ 0 & 0 & 0 & 0 & 0.997 & 0 \end{pmatrix}. \tag{34}$$

This time the bandpass response is adjusted to have a bandwidth of 58 MHz at a center frequency $f_0 = 890$ MHz, given a fractional bandwidth of $F_B = 6.5\%$. After optimization, the parameters of the modulated capacitors are $f_m = 19$ MHz, $\Delta_m = 0.076$, and $\Delta_\varphi = 48°$.

Fig. 7 shows the simulated scattering parameters with increasing number of nonlinear harmonics $N_{har} = 3, 7, 9$. It is evident that the response is inaccurate if only three harmonics are included in the calculations. After increasing further the number of harmonics, the differences among the different simulations reduce considerably, especially for the reflection characteristic and the forward transmission coefficient. We have verified that including additional harmonics in the simulations leads to negligible variations in the simulated response, which indicates that good convergence is obtained with nine harmonics. As expected, this study shows that more harmonics needs to be used in the numerical simulations when the order of the network increases.

Moreover, it has been previously shown [16], that in this type of modulated resonators only the two first higher order harmonics are important in the nonlinear process. Consequently, the minimum number of harmonics that need to be considered in the numerical simulations should grow, with the number of resonators in the network, according to the rule: $N_{har} = 2(N-1)+1$. Note that the convergence results

presented for the third and fourth order filters, shown in Fig. 6 and Fig. 7, are in agreement with this rule.

The filter shows an almost flat response for the transmission coefficient in the forward direction, having a bandwidth of 40 MHz measured at a return loss of $RL = 12$ dB. The insertion losses in the forward direction are smaller than $IL = 3.3$ dB within the useful passband. Again, these losses correspond to power converted from the fundamental frequency into nonlinear harmonics that is not converted back into the fundamental frequency. The response of the filter shows a strong non-reciprocal behavior in the backward direction. Around the center frequency, the directivity is better than $D_0 = 13.7$ dB in a bandwidth of 26 MHz. In the whole useful passband, the directivity is shown to be better than $D = 9$ dB.

At this point it is interesting to observe that the optimum modulation frequency ($f_m = 19$ MHz) is slightly smaller than the bandwidth of the filter. This condition assures that the two first intermodulation products can be strongly excited, while the generation of higher order intermodulation products are minimized. Also, we emphasize that the response of the filter was optimized to achieve a good trade-off between the isolation level, and the bandwidth where it is achieved. Other optimization criteria are possible, for instance by increasing further the isolation level, at the expense of reducing the bandwidth where this isolation is achieved. For instance we have verified that by decreasing the frequency of the modulation signal to $f_m = 18$ MHz, the directivity increases to $D_0 = 33.1$ dB, although in a narrow bandwidth of only 8.6 MHz. In any case, this example shows that the proposed system offers high flexibility in the characteristics that can be achieved, that could be adapted to many different scenarios.

As validation of the theory presented in this paper, we employ this last filter design to compare our results with those obtained with the commercial tool ADS [33]. Here we remark that the ADS results were obtained using ideal built-in models to implement the time modulated capacitors through (13), combined with the large signal scattering parameters analysis module. In addition, we also check what is the impact of the approximations introduced in order to formulate the frequency independent elements required by the coupling matrix formalism. Essentially, the approximations involve (i) the representation of the harmonic resonators with the frequency invariant susceptances of (29), instead of using the rigorous admittances given in (24); and (ii) the use of frequency independent admittance inverters of (31), instead of the rigorous expressions shown in (30). Fig. 8 compares the filter response using these two different approaches, and using the commercial tool ADS. It can be observed that our theory (solid lines, denoted as 'Rigorous') agrees perfectly with the results obtained with ADS (markers). Small differences can be observed between these two results (ADS, Rigorous), and the results obtained introducing the approximations (dashed lines, denoted as 'CM'). This indicates that the impact of the approximations introduced is indeed small, especially for narrowband filters.

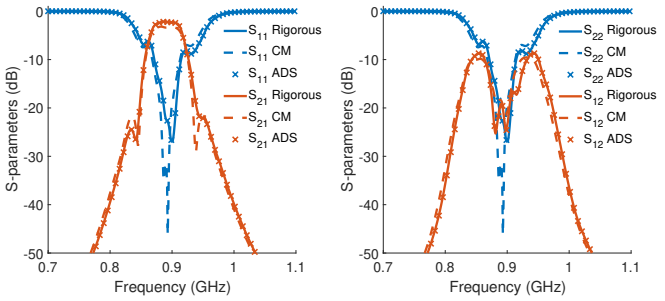

(a) (b)

Fig. 8. Scattering parameters of the fourth order non-reciprocal filter designed in Section IV computed using the commercial tool ADS (cross symbols), the coupling matrix approach introduced in this work with approximations (CM; dashed line) and without approximations (solid lines). Approximations involve the use of (27)-(29) and (31). In both calculations the number of harmonics has been fixed to $N_{har} = 9$.

TABLE I
DIMENSIONS (IN MILLIMETERS) OF THE FABRICATED 3RD-ORDER FILTER (SEE FIG. 9).

W_1	W_2	W_3	S_1	S_2	S_3	h_1	l_1	l_2
50	3.44	3	2.66	0.36	0.22	11.3	153	72
l_3	l_4	l_5	l_6	l_7	l_8	l_9	Φ_1	Φ_2
31.3	69	100	17	31.95	15.5	20.4	1.8	1

V. PRACTICAL REALIZATION

In this Section we present the fabrication and measurement of the two previously designed non-reciprocal filters, implemented in microstrip technology. Fig. 9 and Fig. 10 show the details of the filters together with pictures of the manufactured prototypes. It can be observed that the top metallization layer contains the input/output RF feeding lines and that the resonators are realized using quarter wavelength transmission lines terminated on one side with a via-hole connected to a varactor. On the bottom metallization layer the ground plane of the microstrip line is modified to feed the various varactors (from Skyworks, model SMV1234) with the corresponding modulating signals using coplanar waveguides. In the figures we also show the positions where the varactors are soldered in the board. Note that a choke lumped inductor of value 180 nH is incorporated to increase the isolation between the signals oscillating at f_0 and f_m. It should be emphasized that this implementation enforces that the RF and modulating signals are supported on different planes of the substrates which significantly increases the isolation between them (> 30 dB). The substrate material used for the fabrication is Rogers RT/duroid 6035 HTC with a relative dielectric constant $\epsilon_r = 3.5$ and a thickness of 1.524 mm. The final dimensions of the fabricated prototypes are collected in Table I and Table II for the third and fourth order filters, respectively.

Fig. 11a shows the measured results for the third order filter in the absence of any modulation and compares them with the simulated response using the coupling matrix formalism. Here we should remark that the simulated responses of the filters are all obtained with the theoretical analysis

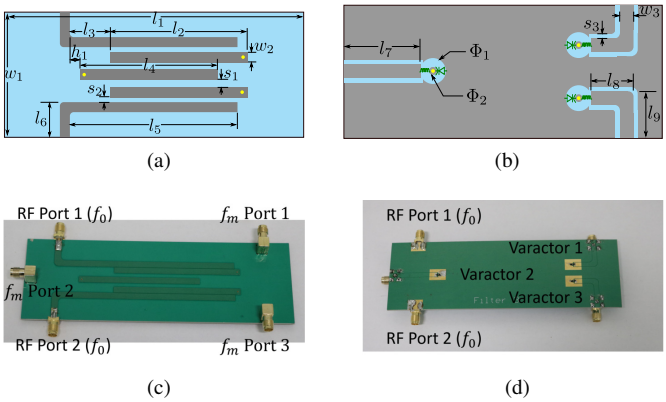

(a) (b) (c) (d)

Fig. 9. Geometry of the third order filter designed in microstrip technology. (a) Detail of the top metalization layer. (b) Detail of the bottom metalization layer. Panels (c)-(d) show a picture of the top and bottom metalization layers of the fabricated prototype, respectively.

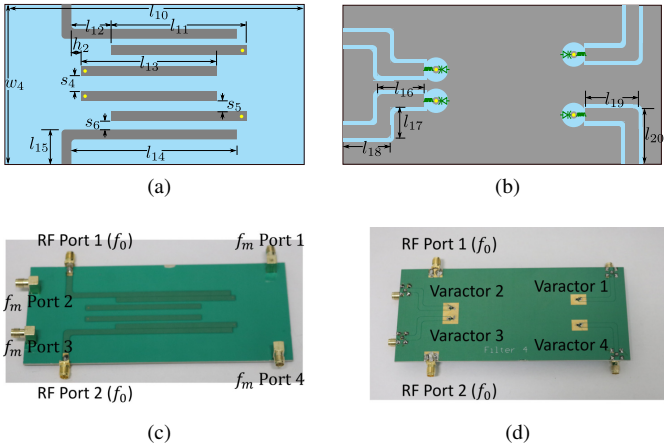

(a) (b) (c) (d)

Fig. 10. Geometry of the fourth order filter designed in microstrip technology. (a) Detail of the top metalization layer. (b) Detail of the bottom metallization layer. Panels (c)-(d) show a picture of the top and bottom metalization layers of the fabricated prototype, respectively.

TABLE II
DIMENSIONS (IN MILLIMETERS) OF THE FABRICATED 4TH-ORDER FILTER (SEE FIG. 10).

W_4	S_4	S_5	S_6	h_2	l_{10}	l_{11}	l_{12}
70	4.56	2.21	0.21	9.3	160	73	27.8
l_{13}	l_{14}	l_{15}	l_{16}	l_{17}	l_{18}	l_{19}	l_{20}
70.3	98.1	23.4	22.5	14	17	25.5	26.9

presented in Section III. In addition, it can be observed in the measured response some deviations with respect to the response of the designed prototype shown in Fig. 6. The differences are mainly due to the insertion losses within the passband, which are around $IL = 2.8$ dB, and to some parasitic cross couplings that were not taken into account during the initial design. These two factors have been included in the simulated responses obtained with the coupling matrix formalism derived in this work, shown in Fig. 11. Losses in the resonators are modeled with an additional resistor connected in parallel. The response show in Fig. 11a is used to extract the unloaded quality factors of the resonators, giving $Q_U = 114$. This unloaded quality factor is small, but within the range achievable in planar technology [34], and especially when using microstrip line printed resonators. In addition, we have found that the drop of selectivity in the lower side of the passband is mainly due to a non negligible cross coupling between the ports and the second resonator, giving normalized coupling factors or $M_{P_1 2} = M_{2 P_2} = 0.26$. Although of much weaker value, there is also a small parasitic coupling between the first and third resonator, which is modeled with a normalized coupling factor of $M_{13} = 0.09$. It can be observed that the agreement between measured and simulated results are very good, once losses and parasitic couplings are included in the derived coupling matrix formalism.

Fig. 11b presents the measured versus simulated results when the modulating signal is applied to the varactors and the filter is excited from the first port. It can be observed that the filter behaves as in the unmodulated case, with increased losses of around $IL = 4.5$ dB that account for both dissipation effects and the power converted into nonlinear harmonics. The useful bandwidth measured at a return loss level of $RL = 11$ dB is 45 MHz. Fig. 11c shows the response of the prototype when it is excited from the second port. The filtering response is suppressed and instead the device behaves as an isolator that attenuates all incoming power. Maximum non-reciprocity is achieved at the center of the passband with a directivity of $D_0 = 13.8$ dB. It should be emphasized that when losses and parasitic cross couplings are included in the coupling matrix model, an excellent agreement is obtained between measured data and numerical simulations.

Measurements corresponding to the fourth order filter are shown in Fig. 12. Fig. 12a plots the response of the filter before introducing the modulating signal and compares it with respect to the response of the ideal circuit. Again the bandwidth and the ripple level obtained within the passband are very similar. Measured results exhibit a perfectly constant equi-ripple response, since the resonant frequencies of the resonators are slightly tuned with constant voltages applied to the varactors. The insertion losses due to dissipation effects in the resonators and in the varactors are slightly larger than in the previous filter, obtaining a minimum level of $IL = 3.2$ dB that slowly increases towards the end of the passband. The insertion losses measured in the unmodulated case (Fig. 12a) were used again to extract the unloaded quality factor of the resonators, obtaining essentially the same value as in the previous example. This is something to be expected, since the same resonators as before were used in this second prototype, and the same technology was used for manufacturing. In any case, this also shows high repeatability of the employed manufacturing process.

Measured results again show a small drop in selectivity as compared to the designed response of Fig. 7, especially in the lower side of the passband. Once more we found that this is due to parasitic cross couplings not taken into account during the initial design process. In the comparison shown in Fig. 12, we can observe good agreement between measured and simulated responses when losses and parasitic couplings are included in the derived model. Again, we found that the

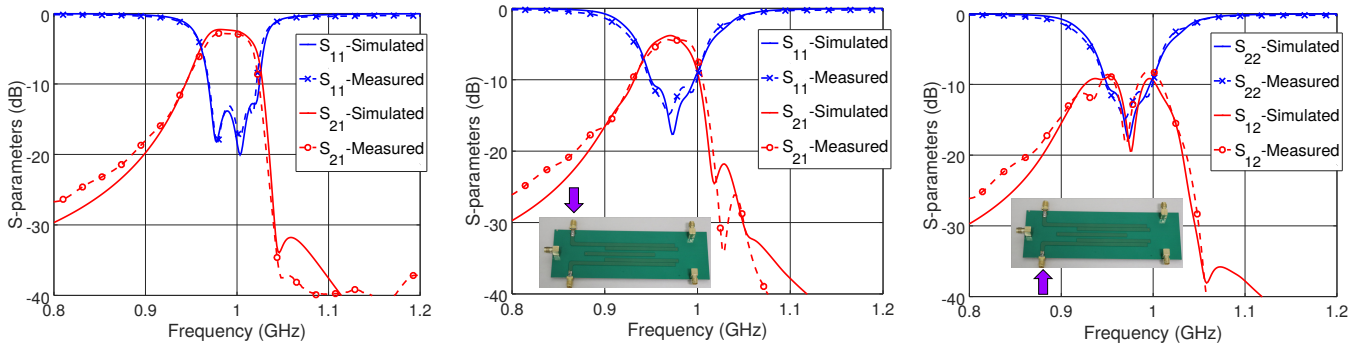

(a) (b) (c)

Fig. 11. Measured response of the manufactured third order non-reciprocal filter and comparison with respect to the numerical results obtained with the proposed technique. In our numerical simulations, losses and parasitic cross couplings have been included in the coupling matrix approach as described in the text. (a) Unmodulated case related to the reciprocal response of the filter in which $S_{11} = S_{22}$ and $S_{12} = S_{21}$. (b)-(c) Response obtained when the modulating signal is applied to the varactors and the filter is excited (shown in the inset using a magenta arrow) from the first (b) and the second (c) port.

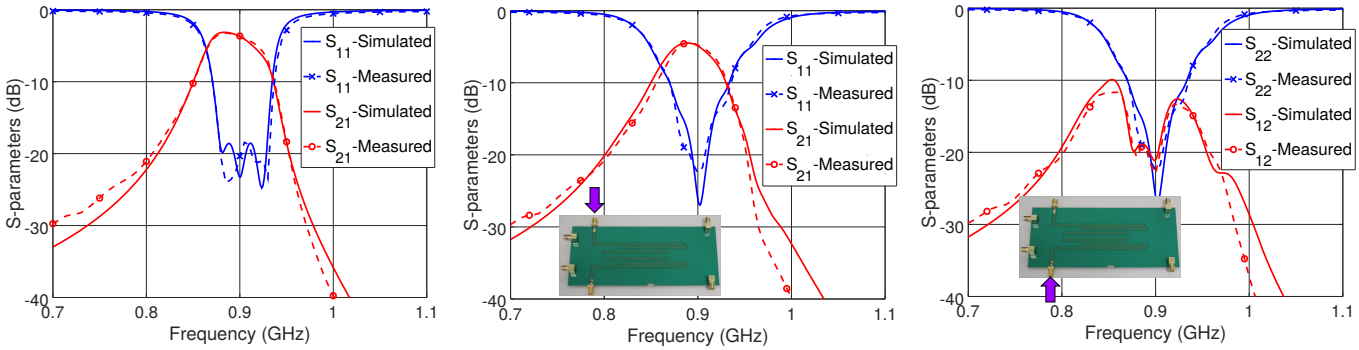

(a) (b) (c)

Fig. 12. Measured response of the manufactured fourth order non-reciprocal filter and comparison with respect to the numerical results obtained with the proposed technique. In our numerical simulations, losses and parasitic cross couplings have been included in the coupling matrix approach as described in the text. (a) Unmodulated case related to the reciprocal response of the filter in which $S_{11} = S_{22}$ and $S_{12} = S_{21}$. (b)-(c) Response obtained when the modulating signal is applied to the varactors and the filter is excited (shown in the inset using a magenta arrow) from the first (b) and the second (c) port.

TABLE III
BASIC ELECTRICAL PERFORMANCES OBTAINED FOR THE TWO MANUFACTURED FILTERS.

	IL (dB)	RL (dB)	D (dB)	F_B (%)
Third order	4.5	11	13.8	4.6
Fourth order	4.4	11	13.6	6.4

strongest parasitic couplings occur between the ports and the closest non contiguous resonators: $M_{P_1 2} = M_{3P_2} = 0.23$ and $M_{P_1 3} = M_{2P_2} = 0.1$. However, non negligible parasitic couplings have also been found between internal resonators: $M_{13} = M_{24} = 0.12$ and $M_{14} = 0.06$.

Fig. 12b presents the measured results obtained from the manufactured prototype when the modulating signal is applied to the varactors and the filter is excited from the first port. The fabricated prototype behaves as a filter with a useful bandwidth of 57 MHz measured at a return loss level of $RL = 11$ dB. With respect to the unmodulated case, the insertion losses in the forward direction have increased to $IL = 4.4$ dB. As in the previous case, the extra losses are due to power converted into nonlinear harmonics that is not converted back to the fundamental frequency. Exciting the device from the second port significantly attenuates the propagating energy. The strong non-reciprocity predicted by the initial simulations is confirmed by the measurements. Around the center frequency of the passband, the directivity is better than $D_0 = 13.6$ dB in a bandwidth of 35 MHz. Across the entire passband, the directivity is always better than $D = 7.2$ dB. In general, very good agreement between measured and simulated responses are obtained when losses and parasitic couplings are included in the derived coupling matrix model. For reference, the basic performances for both manufactured filters are collected in Table III.

Another important characteristic of these devices for many applications is the power handling levels [35]. Even though we have not tested the proposed filters under high power signals, other works [12] have shown that the nonlinear response of varactors and their associated parasitic components are the most critical factors that limit the power handling capabilities of time-modulated circuits. The power handling of the designed devices, then, will primarily depend on the type of varactor used, and on the value of its breakdown voltage [12].

VI. Conclusion

We have presented the analysis of non-reciprocal filters based on time modulated capacitors using a coupling matrix formalism. From the initial topology of the filter, a novel coupling topology using harmonic resonators is first derived. Closed form analytic expressions have been obtained to represent the harmonic resonators with frequency invariant susceptances, thus obtaining the diagonal elements of the traditional coupling matrix. Also, non-reciprocal admittance inverters have been analytically computed to account for the couplings between harmonic resonators, thus obtaining the off-diagonal elements of the coupling matrix. The derived analysis method has been validated with the design and fabrication of third and fourth order filters implemented in microstrip technology. Measured results on the fabricated prototypes, and results obtained with a commercial tool are found to agree well with respect to numerical calculations obtained using the new coupling matrix formulation, thus fully validating the theory presented.

Acknowledgment

Authors are grateful to Rogers Corporation for the generous donation of the dielectrics employed in this work.

References

[1] D. M. Pozar, *Microwave Engineering*. John Wiley and Sons, 1998, ISBN: 0-471-17096-8.

[2] C. Caloz, A. Alu, S. Tretyakov, D. Sounas, K. Achouri, and Z. L. Deck-Leger, "Electromagnetic nonreciprocity," *Phys. Rev. Appl.*, vol. 10, no. 4, p. 047001, 2018.

[3] A. Kord, D. L. Sounas, and A. Alu, "Achieving full-duplex communication: Magnetless parametric circulators for full-duplex communication systems," *IEEE Microw. Mag.*, vol. 19, no. 1, pp. 84–90, Janaury 2018.

[4] T. Kodera, D. L. Sounas, and C. Caloz, "Magnetless nonreciprocal metamaterial (mnm) technology: Application to microwave components," *IEEE Trans. Microw. Theory Techn.*, vol. 61, no. 3, pp. 1030–1042, March 2013.

[5] R. Fleury, D. L. Sounas, C. F. Sieck, M. R. Haberman, and A. Alu, "Sound isolation and giant linear nonreciprocity in a compact acoustic circulator," *Science*, vol. 343, no. 6170, pp. 516–519, 2014.

[6] N. A. Estep, D. L. Sounas, J. Soric, and A. Alu, "Magnetic-free non-reciprocity and isolation based on parametrically modulated coupled resonator loops," *Nat. Phys.*, vol. 10, no. 12, pp. 923–927, December 2014.

[7] N. A. Estep, D. L. Sounas, and A. Alu, "Magnetless microwave circulators based on spatiotemporally modulated rings of coupled resonators," *IEEE Trans. Microw. Theory Techn.*, vol. 64, no. 2, pp. 502–518, February 2016.

[8] N. Reiskarimian and H. Krishnaswamy, "Magnetic-free non-reciprocity based on staggered commutation," *Nat. Commun.*, vol. 7, no. 4, p. 11217, April 2016.

[9] N. Reiskarimian, J. Zhou, and H. Krishnaswamy, "A cmos passive lptv nonmagnetic circulator and its application in a full-duplex receiver," *Nat. Commun.*, vol. 52, no. 5, pp. 1358–1372, May 2017.

[10] T. Dinc, M. Tymchenko, A. Nagulu, D. Sounas, A. Alu, and H. Krishnaswamy, "Synchronized conductivity modulation to realize broadband lossless magnetic-free non-reciprocity," *Nat. Commun.*, vol. 8, p. 759, October 2017.

[11] A. Kord, D. L. Sounas, and A. Alu, "Magnet-less circulators based on spatiotemporal modulation of bandstop filters in a delta topology," *IEEE Trans. Microw. Theory Techn.*, vol. 66, no. 2, pp. 911–926, February 2018.

[12] ——, "Pseudo-linear time-invariant magnetless circulators based on differential spatiotemporal modulation of resonant junctions," *IEEE Trans. Microw. Theory Techn.*, vol. 66, no. 6, pp. 2731–2745, June 2018.

[13] Y. Yu, G. Michetti, A. Kord, D. Sounas, F. V. Pop, M. P. P. Kulik, Z. Qian, A. Alu, and M. Rinaldi, "Magnetic-free radio frequency circulator based on spatiotemporal commutation of mems resonators," in *IEEE Microelectromech. Syst.*, January 2018, pp. 154–157.

[14] Z. Yu and S. Fan, "Complete optical isolation created by indirect interband photonic transitions," *Nat. Photonics*, vol. 3, p. 91, January 2008.

[15] H. Lira, Z. Yu, S. Fan, and M. Lipson, "Electrically driven nonreciprocity induced by interband photonic transition on a silicon chip," *Phys. Rev. Lett.*, vol. 109, p. 033901, July 2012.

[16] S. Qin, Q. Xu, and Y. E. Wang, "Nonreciprocal components with distributedly modulated capacitors," *IEEE Trans. Microw. Theory Techn.*, vol. 62, no. 10, pp. 2260–2272, October 2014.

[17] J. Chang, J. Kao, Y. Lin, and H. Wang, "Design and analysis of 24-ghz active isolator and quasi-circulator," *IEEE Trans. Microw. Theory Techn.*, vol. 63, no. 8, pp. 2638–2649, August 2015.

[18] M. M. Biedka, R. Zhu, Q. M. Xu, and Y. E. Wang, "Ultra-wide band non-reciprocity through sequentially-switched delay lines," *Scientific Reports*, vol. 7, p. 40014, January 2017.

[19] D. Correas-Serrano, A. Alu, and J. S. Gomez-Diaz, "Magnetic-free nonreciprocal photonic platform based on time-modulated graphene capacitors," *Phys. Rev. B*, vol. 8, p. 165428, 2018.

[20] D. L. Sounas, J. Soric, and A. Alu, "Broadband passive isolators based on coupled nonlinear resonances," *Nat. Electron.*, vol. 1, pp. 113–119, February 2018.

[21] D. C. Serrano, J. G. Diaz, D. Sounas, Y. Hadad, A. A. Melcon, and A. Alu, "Non-reciprocal graphene devices and antennas based on spatio-temporal modulation," *IEEE Antennas Wireless Propag. Lett.*, vol. 15, no. 6, pp. 1529–1533, June 2016.

[22] T. Kodera, D. L. Sounas, and C. Caloz, "Breaking temporal symmetries for emission and absorption," *Proc. Natl. Acad. Sci.*, vol. 113, p. 3471, 2016.

[23] S. Taravati and C. Caloz, "Mixer-duplexer-antenna leaky-wave system based on periodic space-time modulation," *IEEE Trans. Antennas Propag.*, vol. 65, no. 2, pp. 442–452, February 2017.

[24] X. Wu, X. Liu, M. D. Hickle, D. Peroulis, J. S. Gomez-Diaz, and A. A. Melcon, "Isolating bandpass filters using time-modulated resonators," *IEEE Trans. Microw. Theory Techn.*, vol. 67, no. 6, pp. 2331–2345, June 2019.

[25] R. J. Cameron, "Advanced coupling matrix synthesis techniques for microwave filters," *IEEE Trans. Microw. Theory Techn.*, vol. 51, no. 1, pp. 1–10, Jan. 2003.

[26] R. J. Cameron, C. M. Kudsia, and R. R. Mansour, *Microwave Filters for Communication Systems*. Hoboken, New Jersey: Wiley, 2007, ISBN: 978-0-471-45022-1.

[27] L. A. Pipes, "Matrix analysis of linear time-varying circuits," *J. of Appl. Phys.*, vol. 25, no. 9, pp. 1179–1185, September 1952.

[28] K. D. Dikshit, "An analysis of time-varying circuits," *Int. J. of Electron.*, vol. 35, no. 4, pp. 453–460, April 1873.

[29] P. Soto, E. Tarin, V. Boria, C. Vicente, J. Gil, and B. Gimeno, "Accurate synthesis and design of wideband inhomogeneous inductive waveguide filters," *IEEE Trans. Microw. Theory Techn.*, vol. 58, no. 8, pp. 2220–2230, August 2010.

[30] F. M. Vannin, D. Schmitt, and R. Levy, "Dimensional synthesis for wide-band waveguide filters and diplexers," *IEEE Trans. Microw. Theory Techn.*, vol. 52, no. 11, pp. 2488–2495, November 2004.

[31] S. Darlington, "Linear time-varying circuits - matrix manipulations, power relations, and some bounds on stability," *The Bell System Technical Journal*, vol. 42, no. 6, pp. 2575–2608, November 1963.

[32] C. F. Kurth, "Steady-state analysis of sinusoidal time-variant networks applied to equivalent circuits for transmission networks," *IEEE Trans. Circuits Syst.*, vol. CAS-24, no. 11, pp. 610–624, November 1977.

[33] Keysight Technologies, *ADS - Advanced Design System*, EEsof, Santa Rosa, CA, USA, 2019. [Online]. Available: https://www.keysight.com

[34] Y.-Y. Zhu, Y.-L. Li, and J.-X. Chen, "A novel dielectric strip resonator filter," *IEEE Microw. Wireless Compon. Lett.*, vol. 7, pp. 591–593, July 2018.

[35] L.-S. Wu, X.-L. Zhou, W.-Y. Yin, M. Tang, and L. Zhou, "Characterization of average power handling capability of bandpass filters using planar half-wavelength microstrip resonators," *IEEE Microw. Wireless Compon. Lett.*, vol. 19, no. 11, pp. 686–688, November 2009.

Alejandro Alvarez Melcon (M'99-SM'07) was born in Madrid, Spain, in 1965. He received the Telecommunications Engineer degree from the Technical University of Madrid (UPM), Madrid, Spain, in 1991, and the Ph.D. degree in electrical engineering from the Swiss Federal Institute of Technology, Lausanne, Switzerland, in 1998. In 1988, he joined the Signal, Systems and Radiocommunications Department, UPM, as a research student, where he was involved in the design, testing, and measurement of broad-band spiral antennas for electromagnetic measurements support (EMS) equipment. From 1991 to 1993, he was with the Radio Frequency Systems Division, European Space Agency (ESA/ESTEC), Noordwijk, The Netherlands, where he was involved in the development of analytical and numerical tools for the study of waveguide discontinuities, planar transmission lines, and microwave filters. From 1993 to 1995, he was with the Space Division, Industry Alcatel Espacio, Madrid, Spain, and was also with the ESA, where he collaborated in several ESA/European Space Research and Technology Centre (ESTEC) contracts. From 1995 to 1999, he was with the Swiss Federal Institute of Technology, École Polytechnique Fédérale de Lausanne (EPFL), Lausanne, Switzerland, where he was involved with the field of microstrip antennas and printed circuits for space applications. In 2000, he joined the Technical University of Cartagena, Spain, where he is currently developing his teaching and research activities. Dr. Alvarez Melcón was de recipient of the *Journée Internationales de Nice Sur les Antennes* (JINA) Best Paper Award for the best contribution to the JINA'98 International Symposium on Antennas, and the *Colegio Oficial de Ingenieros de Telecomunicación* (COIT/AEIT) Award to the best Ph.D. thesis in basic information and communication technologies.

Xiaohu Wu (M'15-SM'19) was born in Hubei, China, in 1987. He received the B.Eng. degree in infor- mation engineering and Ph.D. degree in electro- magnetic fields and microwave technology from the South China University of Technology, Guangzhou, China, in 2008 and 2013, respectively. His Ph.D. dissertation concerned the exploration of multimode resonators and their applications to filter design. From 2013 to 2014, he was an Engineer with the East China Research Institute of Electronic Engineering (ECRIEE), Hefei, China, where he was involved in scalable active arrays. In 2015, he joined the School of Electronic and Information Engineering, Nanjing University of Information Science and Technology, Nanjing, China, as an Assistant Professor. Since 2017, he has been a Post-Doctoral Researcher with the Department of Electrical and Computer Engineering, University of California at Davis, Davis, CA, USA. His current research interests include time-varying nonreciprocal devices and absorptive circuit design.

Jiawei Zang received the Ph.D. degree in electrical engineering from the Beijing Institute of Technology, Beijing, China, in 2019. From September 2017 to November 2018, he was a visiting student in the Department of Electrical and Computer Engineering, University of California, Davis. His research interests include antennas, filters, and nonreciprocal components.

Xiaoguang (Leo) Liu (M'10-SM'16) received the bachelors degree from Zhejiang University, Hangzhou, China, in 2004, and the Ph.D. degree from Purdue University, West Lafayette, IN, USA, in 2010. In 2011, he joined the Department of Electrical and Computer Engineering, University of California at Davis, Davis, CA, USA, as an Assistant Professor, and was promoted to an Associate Professor in 2017. At the University of California at Davis, his research group is currently investigating various aspects of cutting-edge high-frequency and high-speed circuit and system designs.

J. Sebastian Gomez-Diaz (M'11-SM'16) was born in Ontur, Spain, in 1983. He received the Telecommunications Engineer and Ph.D. degrees in electrical engineering from the Technical University of Cartagena (UPCT), Cartagena, Spain, in 2006 and 2011, respectively. In 2006, he joined the Telecommunication and Electromagnetic Group (GEAT), UPCT, as a Research Assistant. During the development of his Ph.D., he held visiting research positions with the cole Polytechnique de Montral, Montreal, QC, Canada, and the Fraunhofer Institute for High Frequency Physics and Radar Techniques, Germany. From 2011 to 2014, he was a Post-Doctoral Fellow with the cole Polytechnique Fdrale de Lausanne (EPFL), Lausanne, Switzerland. From 2014 to 2016, he continued his post-doctoral work with the Metamaterials and Plasmonic Research Laboratory, The University of Texas at Austin, Austin, TX, USA. He is currently an Assistant Professor with the Electrical and Computer Engineering Department, University of California at Davis, Davis, CA, USA. His current research interests include multidisciplinary areas of electromagnetic wave propagation and radiation, metamaterials and metasurfaces, plasmonics, 2-D materials, nonreciprocal and nonlinear phenomena, and other emerging topics on applied electromagnetics and nanotechnology. Dr. Gmez-Daz was a recipient of the Best Ph.D. Thesis Award from the Technical University of Cartagena, the Colegio Oficial de Ingenieros de Telecomunicacin (COIT/AEIT) Award to the Best Spanish Ph.D. Thesis in basic information and communication technologies in 2011, the FP7 Marie Curie Fellowship from the European Commision in 2012, the Raj Mittra Award from the 2015 IEEE Antennas and Propagation Society, the Young Scientist Award of the 2015 URSI Atlantic RadioScience Conference, the 2017 Leopold Felsen Award for Excellence in Electrodynamics, and the 2018 NSF CAREER Award. He serves as a Reviewer for several journals on antennas, microwaves/THz, and physics.